Supplement of Weather Clim. Dynam., 7, 1385–1403, 2026
https://doi.org/10.5194/wcd-7-1385-2026-supplement

Supplement of

Austral summer MJO forecast skill in S2S models: decadal shifts and their drivers

Raina Roy et al.

Correspondence to: Raina Roy (raina.roy@monash.edu)

Supplementary Information

VAR model

We employ a Vector Autoregressive (VAR) model, following Marshall et al. (2016) and Maharaj & Wheeler (2005), to establish a baseline for MJO predictability independent of dynamical model complexities. The model predicts future RMM1 and RMM2 indices using their lagged values through the coupled equations:

VAR System:

$RMM1(t) = \alpha_1 + \beta_{11}RMM1(t\text{-}1) + \beta_{12}RMM2(t\text{-}1) + \varepsilon_1(t)$

$RMM2(t) = \alpha_2 + \beta_{21}RMM1(t\text{-}1) + \beta_{22}RMM2(t\text{-}1) + \varepsilon_2(t)$

Where:

- α1, α2 are intercept terms,
- βij are the coefficients quantifying the influence of lagged RMM1 and RMM2,
- $\varepsilon_1(t)$, ε2(t) are residuals (white noise).

The coefficients (α, β) are estimated using multivariate (multiple) linear regression on historical observations. They are computed separately for each period (e.g., 1981–1998 and 1999–2018) to allow for possible changes in the system's dynamics over time. The equations of the model used for our study are shown below:

For the first period (1981-1998):

$RMM1_t=0.9450\ (RMM1_{t-1}) - 0.1131(RMM2_{t-1})$

$RMM2_t=0.1211\ (RMM1_{t-1}) +0.9820(RMM2_{t-1})$

For the second period (1999-2018):

$RMM1_t= 0.9405\ (RMM1_{t-1}) - 0.1088(RMM2_{t-1})$

$RMM2_t=0.1352\ (RMM1_{t-1}) + 0.9824\ (RMM2_{t-1})$

Bivariate Anomaly Correlation

The bivariate anomaly correlation is estimated using the following formula:

$$\mathrm{COR}\,(\tau) = \frac{\sum_{t=1}^{N} \; [\mathrm{RMM1(t)\,rmm1(t,\tau)} + \mathrm{RMM2(t)\,rmm2(t,\tau)}]/}{\sqrt{(\sum_{t=1}^{N} \; [\mathrm{rmm1(t,\tau)}^{\,2} + \mathrm{rmm2(t,\tau)}^{\,2}])}\,\sqrt{(\sum_{t=1}^{N} \; [\mathrm{RMM1(t)}^{\,2} + \mathrm{RMM2(t)}^{\,2}])}}$$

Here, RMM1 and RMM2 are observed MJO indices, and rmm1 and rmm2 are forecasted MJO indices.

MJO amplitude is computed using the following formula:

$$\mathrm{MJO\ Amplitude\ obs\ (t)} = \sqrt{(\sum_{t=1}^{N} \quad [\mathrm{RMM1(t)}^{\,2} + \mathrm{RMM2(t)}^{\,2}])}$$

$$\mathrm{MJO\ Amplitude\ model\ (t,\tau)} = \sqrt{(\sum_{t=1}^{N} \quad [\mathrm{rmm1(t,\tau)}^{\,2} + \mathrm{rmm2(t,\tau)}^{\,2}])}$$

MJO Skill Index Calculation Method

1. Bivariate Correlation Computation

   For each initialisation date (12 start times per DJF season), calculate the 40-day lead bivariate anomaly correlation (B. Corr) between:
   a. Observed RMM1/RMM2 indices (OBS)
   b. Forecasted rmm1/rmm2 indices (FCST)
2. 15–25 Day Skill Averaging

   a. For each year, compute the mean skill index by averaging correlations across lead times of 15–25 days.
3. Temporal Aggregation

   Repeat Steps 1–2 for all austral summer seasons (DJF) across:
   a. Period 1: 1981–1998 (18 years)
   b. Period 2: 1999–2018 (20 years)
4. Multi-Model Analysis

   Apply this method uniformly to:
   a. Dynamical Models: ACCESS-S2, POAMA2, CESM2, GEOS-S2S-2
   b. Statistical Benchmark: VAR model ensuring cross-comparable skill metrics.

MJO Event estimation

MJO events are calculated using a method that differs slightly from that of Wei & Ren (2019). The steps are as follows:

1. Day 0 of the event can begin in any phase of the MJO.
2. The MJO amplitude must remain above 1 for the next seven consecutive days. This criterion helps identify events that have a strong start.
3. Once the first criterion is met, the MJO must progress in an anticlockwise direction to at least two of the following phases. For our analysis, we have considered both propagating and non-propagating MJO events.

Total yearly event count is the total number of MJO events for a given DJF, and the mean duration is the average duration for these MJO events.

Climate Mode	Phase	Years
IOBM	Positive	1982, 1987, 1989, 1990, 1997, 2002, 2009, 2012, 2015, 2018
IOBM	Negative	1981, 1983, 1984, 1985, 1988, 1992, 1996, 1999, 2000, 2003, 2005, 2007, 2010
IOD	Positive	1995, 1997, 1999, 2000, 2006, 2009, 2012, 2016, 2018
IOD	Negative	1982, 1983, 1984, 1991, 1992, 1998, 2004, 2005, 2007, 2010, 2013, 2014, 2015
QBO	Easterly (EQBO)	1981, 1984, 1989, 1991, 1996, 1998, 2001, 2003, 2005, 2007, 2012, 2014
QBO	Westerly (WQBO)	1982, 1985, 1987, 1988, 1990, 1992, 1997, 1999, 2002, 2004, 2006, 2008, 2010, 2013, 2015, 2016
ENSO	El Niño	1982, 1986, 1987, 1990, 1991, 1992, 1994, 1997, 2002, 2003, 2004, 2006, 2009, 2014, 2015, 2018
ENSO	La Niña	1981, 1983, 1984, 1985, 1988, 1995, 1998, 1999, 2000, 2005, 2007, 2008, 2010, 2011, 2016, 2017

Table S1: Years used to construct the composites in Figure 1 for each climate mode and phase. Climate modes are defined as follows: IOBM (Indian Ocean Basin Mode), IOD (Indian Ocean Dipole), QBO (Quasi-Biennial Oscillation), and ENSO (Niño 3.4 index). Years are classified into positive/negative (or easterly/westerly for QBO) phases based on seasonal mean indices exceeding ±0.5 standard deviations for the austral summer (DJF) period. The table provides the sample size and year lists for each composite used in Figure 1, split into two epochs: 1981–1998 and 1999–2018.

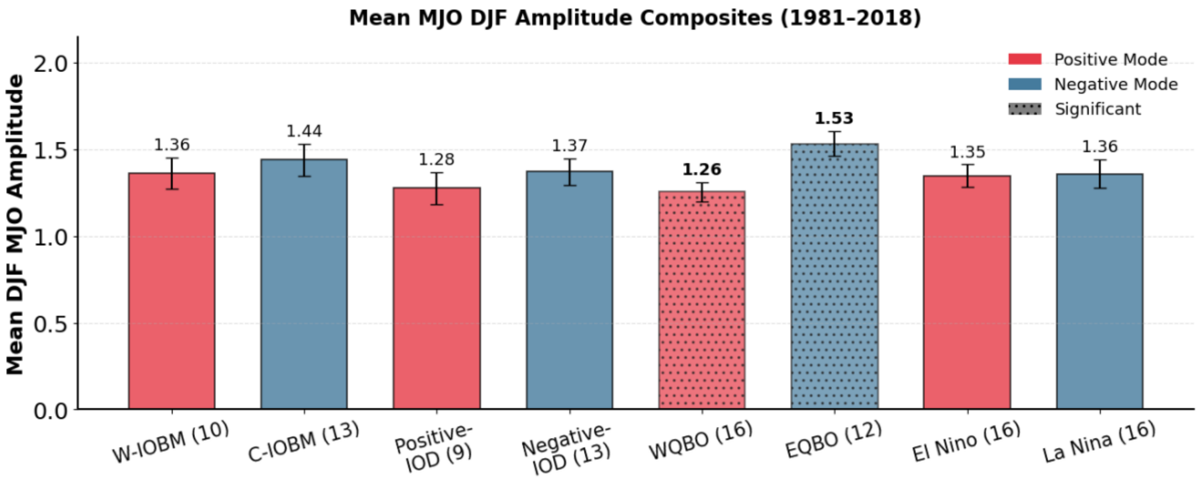

Figure S1: Composite mean amplitude of the MJO across different phases of climate indices—IOBM, IOD, QBO, and Niño 3.4—during austral summer (December-January-February) for the period 1981-2018. The statistical significance of MJO amplitude differences between the positive and negative phases of each index was assessed using a bootstrapping approach (10,000 iterations), in which years were randomly resampled (7 per phase). Stippled bars/bold text above the bars indicate differences exceeding the 90th percentile confidence threshold. Error bars denote the standard error of the mean amplitude in each composite.

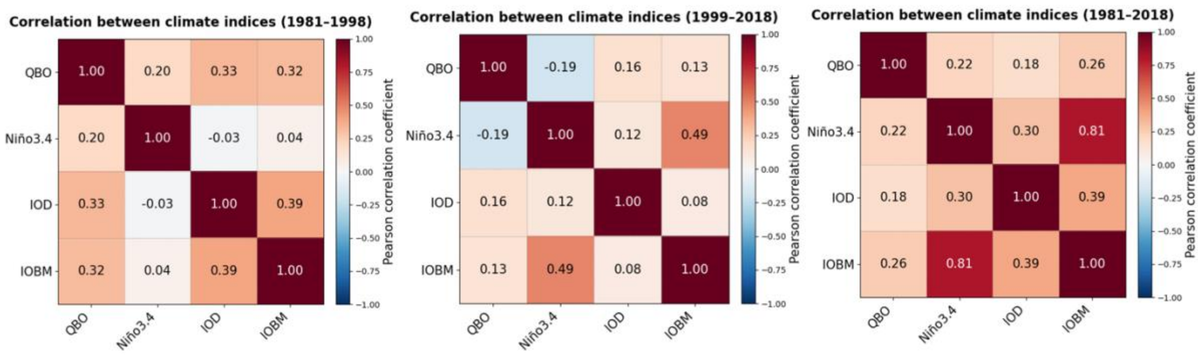

Figure S2: Pearson correlation matrices for QBO, Niño-3.4, IOD, and IOBM during 1981–1998, 1999–2018, and 1981–2018.

Climate Mode	Periods	Correlation between Total observed MJO event count and climate mode index
IOBM	1981-1998	0.11
IOBM	1999-2018	0.38**
IOD	1981-1998	-0.48**
IOD	1999-2018	0.29
QBO	1981-1998	-0.22
QBO	1999-2018	-0.28
ENSO	1981-1998	-0.16
ENSO	1999-2018	0.00
Climate Mode	Periods	Correlation between Mean observed MJO event duration and climate mode index
IOBM	1981-1998	0.12
IOBM	1999-2018	0.09
IOD	1981-1998	0.04
IOD	1999-2018	0.13
QBO	1981-1998	-0.67**
QBO	1999-2018	-0.50**
ENSO	1981-1998	-0.18
ENSO	1999-2018	0.07

Table S2: Correlation coefficients between the MJO event Characteristics (total event count, mean event duration) and observed climate mode indices. Statistical significance was assessed using a two-tailed t-test; ** indicates correlations significant at the 90% confidence level.

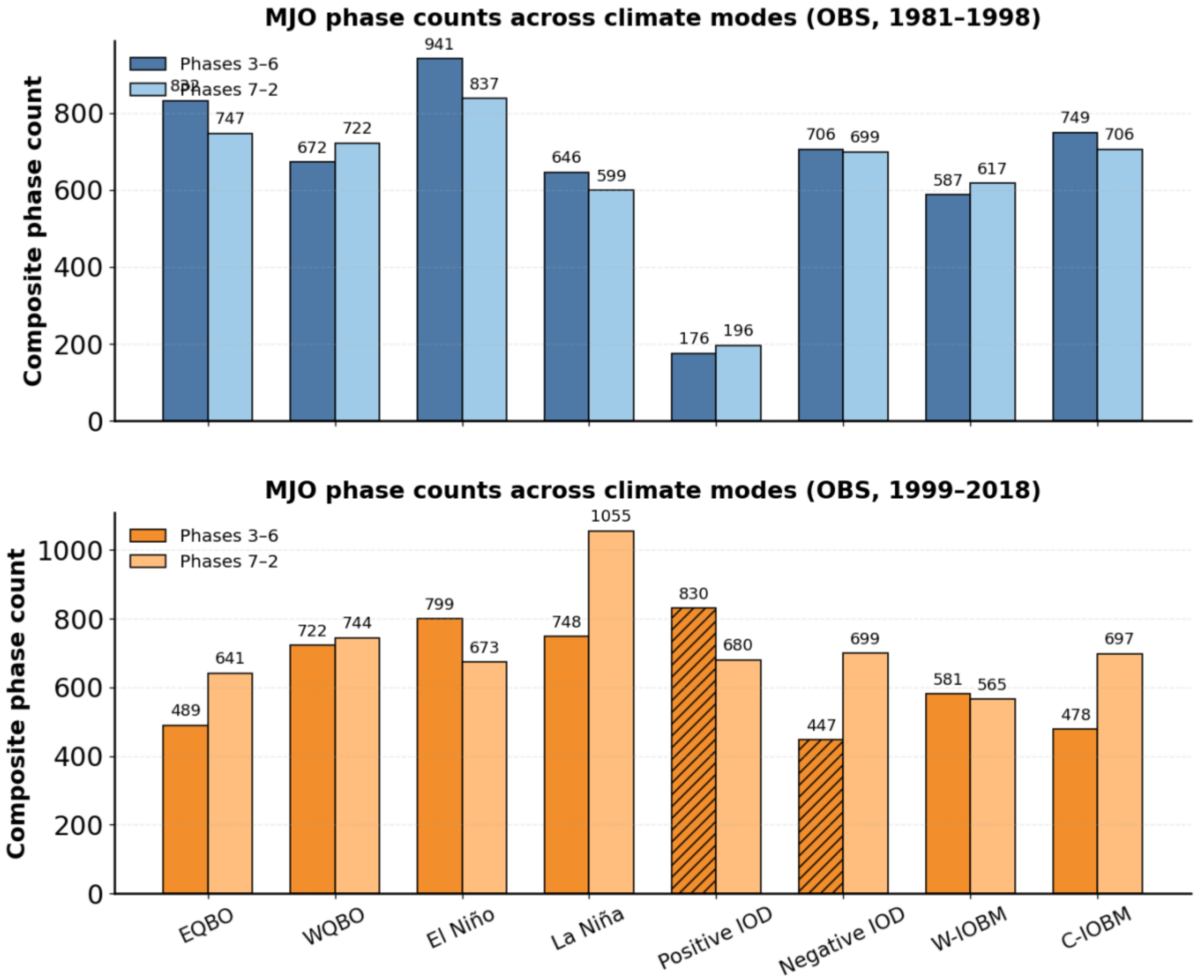

Figure S3: Composite MJO phase frequency distribution for 1981–1998 (row 1) and 1999–2018 (row 2), showing distinct modulation by climate mode phases. Phases 3–6 demonstrate the occurrence in the Eastern Indian Ocean to the Maritime Continent region. Phases 7-2 show the occurrence in the eastern Pacific to the Western Indian Ocean region. Bars with hatching indicate statistically significant differences between opposite phases of each climate mode for a given phase group and period, assessed using a two-sample randomization bootstrap test: for each pair of modes, the observed difference in mean annual composite counts was compared against a null distribution obtained by repeatedly drawing random, equally sized sets of years from all years in that period and recomputing the difference, with significance defined where the two-sided bootstrap p-value is below 0.1.

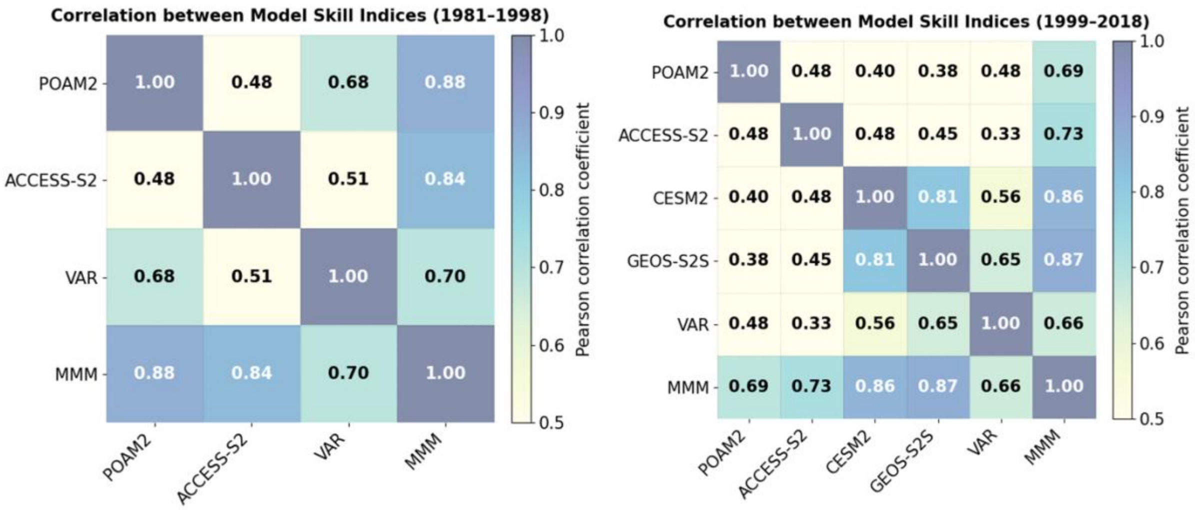

Figure S4: Correlation matrices showing the Pearson correlation coefficients between MJO skill indices for individual models and the multi-model mean (MMM) during two periods: 1981–1998 (left) and 1999–2018 (right). Values along the diagonal correspond to the self-correlation of each model (equal to 1). Off-diagonal values indicate inter-model consistency, with higher values reflecting stronger agreement in MJO skill across models.

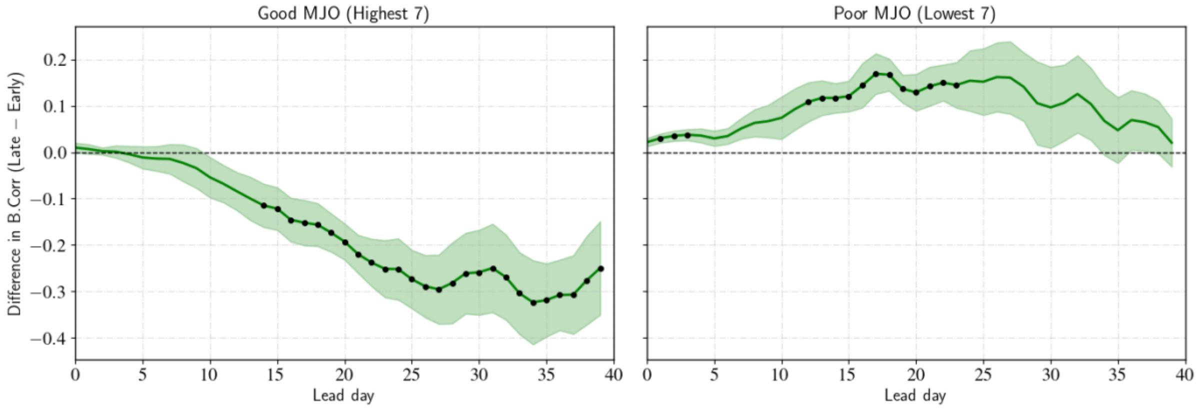

Figure S5: Difference in MJO prediction skill between early and late periods for years with high ("Good MJO," left) and low ("Poor MJO," right) prediction skill. Positive values indicate higher late-period skill relative to early period, shaded areas indicate ±1 standard deviation.

Climate Mode	Periods	Correlations between mean multi model skill index and climate modes
IOBM	1981-1998	-0.21
IOBM	1999-2018	0.17
IOD	1981-1998	-0.36
IOD	1999-2018	0.34
QBO	1981-1998	-0.41**

QBO	1999-2018	-0.46**
ENSO	1981-1998	-0.30
ENSO	1999-2018	0.31

Table S3: Correlation coefficients between the mean multi-model skill index and observed climate mode indices for the periods 1981-1998 and 1999-2018. Statistical significance was assessed using a two-tailed t-test; ** indicates correlations significant at the 90% confidence level.

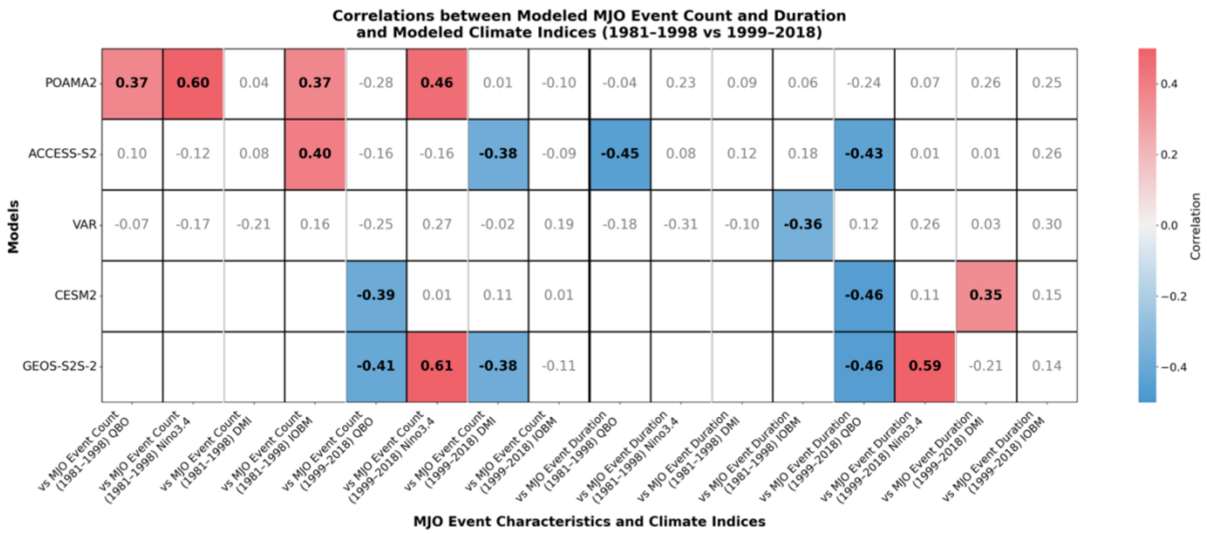

Figure S6: Correlations between modelled MJO event characteristics (event count and duration) and model-derived climate indices (QBO, Niño3.4, DMI, and IOBM) for two periods: 1981–1998 and 1999–2018. Results are shown for POAMA2, ACCESS-S2, VAR, CESM2, and GEOS-S2S-2. Shading indicates the magnitude and sign of the correlation, with red (blue) denoting positive (negative) values. Correlations that are statistically significant at the 95% confidence level are highlighted in bold. This figure is analogous to Figure 6 but uses climate indices estimated from each model rather than from observations, allowing assessment of the sensitivity of MJO–climate mode relationships to the source of the large-scale variability.

References

- Marshall, A. G., Hendon, H. H., and Hudson, D.: Visualizing and verifying probabilistic forecasts of the Madden-Julian Oscillation, Geophys Res Lett, 43, 12278–12286, https://doi.org/10.1002/2016GL071423, 2016.
- Maharaj, E. A. and Wheeler, M. C.: Forecasting an index of the Madden-oscillation, Int J Climatol, 25, 1611–1618, https://doi.org/10.1002/joc.1209, 2005.
- Wei, Y. and Ren, H.-L.: Modulation of ENSO on fast and slow MJO modes during boreal winter, J Climate, 32, 7483–7506, https://doi.org/10.1175/JCLI-D-19-0013.1, 2019.